AIP | Applied Physics Letters

Single atom identification by energy dispersive x-ray spectroscopy

T. C. Lovejoy, Q. M. Ramasse, M. Falke, A. Kaeppel, R. Terborg et al.

Citation: Appl. Phys. Lett. **100**, 154101 (2012); doi: 10.1063/1.3701598
View online: http://dx.doi.org/10.1063/1.3701598
View Table of Contents: http://apl.aip.org/resource/1/APPLAB/v100/i15
Published by the American Institute of Physics.

Single atom identification by energy dispersive x-ray spectroscopy

T. C. Lovejoy,[1] Q. M. Ramasse,[2] M. Falke,[3] A. Kaeppel,[3] R. Terborg,[3] R. Zan,[4] N. Dellby,[1] and O. L. Krivanek[1]
[1]*Nion, 1102 8th St., Kirkland, Washington 98033, USA*
[2]*SuperSTEM Laboratory, STFC Daresbury, Keckwick Lane, Daresbury WA4 4AD, United Kingdom*
[3]*Bruker Nano GmbH, Schwarzschildstr. 12, 12489 Berlin, Germany*
[4]*School of Physics and Astronomy, University of Manchester, Manchester M13 9PL, United Kingdom*

(Received 29 February 2012; accepted 20 March 2012; published online 9 April 2012)

Using aberration-corrected scanning transmission electron microscope and energy dispersive x-ray spectroscopy, single, isolated impurity atoms of silicon and platinum in monolayer and multilayer graphene are identified. Simultaneously acquired electron energy loss spectra confirm the elemental identification. Contamination difficulties are overcome by employing near-UHV sample conditions. Signal intensities agree within a factor of two with standardless estimates. © *2012 American Institute of Physics*. [http://dx.doi.org/10.1063/1.3701598]

Combining real-space imaging of single atoms with elemental identification and spectroscopy at the same spatial resolution is a long-standing goal for analytical instrumentation. To some extent, it has already been achieved with the aberration-corrected scanning transmission electron microscope (STEM). Quantitative annular dark field (ADF) images in which all the atoms are resolved can be used to identify individual light atoms, such as boron, carbon, nitrogen, and oxygen in monolayer materials.[1] Atoms of elements with prominent spectral features have been imaged and identified with single-atom sensitivity by electron energy loss spectroscopy (EELS).[2–6] However, the ADF technique has difficulties in identifying atoms whose projections overlap, and EELS is not optimally sensitive for certain cases, such as third-row transition metals ($_{72}$Hf to $_{85}$At), due to the absence of clear edges in a readily accessible energy range. Energy dispersive x-ray spectroscopy (EDXS) provides another route to elemental identification of such elements, as well as a general method potentially capable of identifying single atoms of nearly all elements.

At the very beginning of quantitative STEM microanalysis, the relative merits of EELS and EDXS were compared in detail by Isaacson and Johnson.[7] EELS was found to have intrinsically better signal/noise ratios than EDXS, with the advantage especially large for light elements. Since then, EELS has become the dominant analytical technique in high-resolution STEM. However, in the last two decades, working aberration correctors have decreased probe sizes in the STEM, while simultaneously increasing the probe current greatly.[8–10] Furthermore, the solid angle obtainable with silicon-drift detectors has been increased recently, and sensitivity to low energy x-rays has been improved. As a result of these developments, EDXS has been able to map atomic columns in crystalline samples at about 2 Å spatial resolution,[11–13] and it seems timely to re-examine the technique's ultimate detection limits. In this paper, elemental identification of individual atoms by EDXS is demonstrated using an aberration-corrected STEM.

The sample used here was chemical vapor deposition (CVD)-grown single-layer graphene on which 2 Å of Pd was deposited by electron-beam evaporation at room temperature. It contained many large areas (10 nm) of pure single layer graphene surrounded by patches of multilayer carbon to which Pd nanoparticles 2–10 nm in size adhered preferentially (no particles were found on pure graphene). There were occasional defects within the graphene lattice including isolated atoms of Si, probably arising from the CVD growth process or from sample preparation (e.g., from glassware). Pt, a common impurity in Pd, was incorporated in or on multilayer graphene areas. Similar results were obtained on another graphene sample.

The individual atoms, located in or on graphene mono- or multilayers, were not altogether stable and were tracked manually, using a small ADF subscan window. Total acquisition times were of the order of 1–5 min, with EDXS and EELS acquired simultaneously. The long acquisition times required contamination-free operation, which was attained by maintaining near-UHV conditions in the sample volume.

The experimental apparatus was a Nion UltraSTEM100 (Ref. 14) at the Daresbury SuperSTEM national facility with a polepiece and sample holder modified to give a side entry Bruker XFlash 5030T silicon drift detector (SDD) a direct view of the sample. The 30 mm^2 detector could be inserted to within ~13 mm of the sample, and we estimate a geometrical efficiency factor of ~0.008 (~0.1 sr). The detector has a thin polymer window which decreases the detector quantum efficiency (DQE), particularly for carbon K x-rays.[15] Unlike the Nion column, the detector cannot be baked at a temperature greater than 60 °C, but a series of valves allows the detector to be mounted, pumped out, and inserted into its operating position without venting the sample area. When inserted, a radial O-ring isolates the detector and sample vaccua; maintaining clean vacuum conditions of $\sim 4 \times 10^{-9}$ Torr in the metal-sealed sample stage that had been baked at 140 °C prior to detector insertion. The microscope is also fitted with a Gatan Enfina electron energy loss spectrometer, which uses O-rings but is bakeable and far enough downstream from the sample chamber so as not to influence the vacuum at the sample.

The STEM probe-forming optics was configured to give 190 pA beam current at 60 keV primary energy, with 30 mrad probe half-angle and a probe size of ~1.4 Å. Atoms of

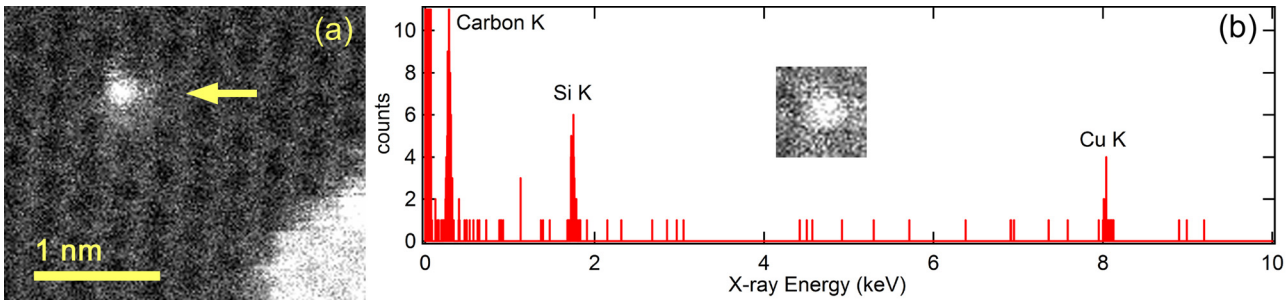

FIG. 1. (a) HAADF image of a single Si impurity atom in monolayer graphene, taken after ~4 min x-ray spectrum acquisition. (b) X-ray spectrum from the Si atom in (a) with (inset) one frame from a simultaneously acquired HAADF centering movie.

interest were first located in high-angle ADF (HAADF) survey scans. A small subscan with ~60 ms frame time was then started over a region $\sim 6 \times 6$ Å^2 (about 10 carbon sites) centered on the atom. EELS and EDXS acquisitions were started at the same time as the subscan. To account for atomic mobility under the beam, which at times caused the atom to jump by Å-sized distances, as well as for slow sample drift, the subscan region was continually recentered on the atom by hand during the entire acquisition time (1–5 min). The subscans were saved and stacked to generate a small movie with each acquisition. The tracking was typically straightforward and can be easily automated in the future, but some atoms were too mobile under the beam for the procedure, which worked best on isolated Si impurity atoms incorporated within the graphene lattice. Finally, a post-acquisition survey image was taken. The most time-consuming part of the experiment was searching for isolated atoms in the graphene lattice which were sufficiently stable. Several different Si and Pt atoms were so studied.

Figure 1 shows a representative Si-atom data set with an HAADF survey image, acquired in ~3 s, an EDX spectrum acquired before the survey image was taken, and one frame from the centering movie. The data are shown with no smoothing, filtering, or processing of any kind. The EDX spectrum shows clear peaks corresponding to the Si K line (1.74 keV) and the carbon K line (0.277 keV). The total acquisition time was 224 s, during which the 1.4 Å probe spent about 10 s directly over the Si atom, and the rest of the time over the carbon sheet. 51 Si K line counts were recorded from 1.617 to 1.890 keV and 115 C K line counts (0.149–0.405 keV). During a 256 s scan of pure graphene, 146 carbon counts were recorded, and 2 counts in the Si energy window. For either spectrum, ~20 copper-K counts (~8 keV) were recorded, probably due to scattered electrons causing emission from the Cu grid the graphene film was supported on. No other peaks were apparent over the entire 0–20 keV detection window.

Figure 2 shows an EEL spectrum acquired simultaneously with the EDX spectrum of Fig. 1. The actual electron count is shown, worked out using an experimentally determined conversion efficiency of 5.0 CCD counts per detected electron. The EELS energy dispersion was set to 0.7 eV/channel and there were 1340 channels on the EELS CCD used to detect the dispersed spectrum. The Si $L_{2,3}$ edge (~100 eV) is clearly visible even before background subtraction, and the carbon K edge (284 eV) is also prominent. The background-subtracted Si $L_{2,3}$ edge signal, integrated over a 100 eV window starting at the edge, has $\sim 6.5 \times 10^6$ electrons, and the background-subtracted C K edge, also integrated over 100 eV, has about 8.1×10^6 electrons. Comparison of the EDX and EEL spectra reveals that the relative background is much smaller with EDX, but that after background subtraction, the EEL spectrum has much better statistics. (It should be noted that the noise level in the EEL spectrum of Fig. 2 is not fundamental to the technique. The spectrum was read out every second during the acquisition, and when summing the partial spectra, an automatic dark current subtraction routine introduced noise greatly in excess of the expected shot noise.)

A similar data set to Figs. 1 and 2 was acquired for a single Pt atom on 3-layer graphene. An HAADF survey image, an EDX spectrum, and a centering image are shown in Fig. 3. In the 245 s spectrum acquisition, during which the probe spent about 11 s over the Pt atom, there were 374 carbon-K counts, 206 Pt-M counts (~2 keV), 61 Pt L-alpha counts (9.4 keV), 45 Pt L-beta counts (11.07 keV), 49 Si-K counts, 45 Fe counts (6.4 keV), 48 Co counts (6.9 keV), and 208 Cu K counts. The carbon signal is larger, roughly in proportion to the increased thickness relative to the spectrum from a monolayer. The system peak from the copper is ~10 times larger, and system peaks from the polepiece (the only Fe or Co in the sample area) are also present. The increased intensity of the system peaks, compared to the Si atom spectrum, is partly due to the ~3× thicker carbon substrate, and mostly due to the increased scattering from the Pt atom.

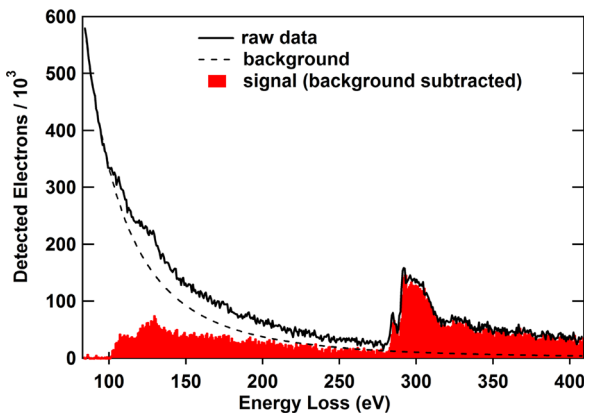

FIG. 2. EEL spectrum simultaneously acquired with Fig. 1(b) showing (solid black) the raw spectrum, (dashed line) the background, and (red fill) the signal after background subtraction. The Si $L_{2,3}$ edge at 100 eV and carbon K edge at 284 eV are clearly visible.

The EDX spectrum from the heavy atom clearly identifies it as a Pt atom. The EEL spectrum (not shown), on the other hand, is difficult to use for elemental identification. Without the clue from EDXS that the atom is Pt, one would have a difficult time noticing the subtle Pt, O, and N edges around 60 eV, which can only be revealed with careful background subtraction using a graphene reference spectrum. Likewise, the EELS M edges at 2.4 keV could be difficult to find without knowing where to look beforehand. The EEL spectrum did play a useful role: it showed no evidence of Cu, Fe, or Co, and thereby confirmed that the presence of peaks from these elements in the x-ray spectrum was due to system background. But this did not change the finding that Pt (Z = 78) was more easily identified by EDXS.

It is instructive to compare the experimental count rates with those expected from first principles for the purpose of understanding the fundamental limits of single atom identification by EDXS or EELS. The count rate, R, of x-rays detected per second per atom when scanning the beam over an area A is given by

$$R = [n^*\sigma/A]^*[\omega^* G^* DQE], \quad (1)$$

where n is the beam current in electrons/second, σ is the cross section for the particular atom and shell being studied (e.g., Si K-shell), ω is the fluorescence yield, G is the geometrical efficiency accounting for the finite fraction of the total solid angle subtended by the detector, and DQE is the probability that an x-ray of the relevant energy impinging on the detector will be detected. The first set of square braces highlights an important quantity, the number of ionizations of the given shell per second. If all energy loss electrons are collected, this is the EELS signal. However, not all the electrons are accepted into the electron spectrometer, and the edge signal is integrated over a finite range of energy losses. When quantifying the EELS signal, this is taken into account by replacing the total cross section, σ, in Eq. (1) by σ_p, the partial cross section for the given collection efficiency and energy window. For efficiently coupled spectrometers that are able to accept >90% of the inelastically scattered electrons, as was the case here, and reasonably sized energy windows, $\sigma_p \sim 0.5\,\sigma$. The second set of square braces is the factor by which the EDXS signal is smaller than the total EELS signal. The cross sections, fluorescence yield, and DQE for the carbon K-shell are 3.2×10^{-4} Å^2,[16] ~0.0027,[17] and 0.37,[15] respectively; for the Si K-shell they are 3.4×10^{-5} Å^2,[16] ~0.047,[18] and 0.71;[15] and for the Pt M shell (M_α plus M_β) they are $\sim 2.4 \times 10^{-4}$ Å^2,[16,19] ~0.025,[20] and 0.73.[15] Note that while σ and ω are physical constants, the DQE curve and the geometrical factor, G, depend on the details of the detector, especially the presence or absence of windows in front of the detector, how close the SDD can be brought to the sample, and the size of the SDD. For this experiment, $G \sim 0.008$, giving $\omega^* G^* DQE = 8.0 \times 10^{-6}$ for the carbon K x-rays, 2.7×10^{-4} for the Si K x-rays, and 1.5×10^{-4} for the Pt M x-rays.

The relevant quantity for comparison between different systems is the maximum count rate that results when the probe is centered over the atom of interest. The experimental maximum count rate is readily obtained by multiplying the measured count rate by the ratio of the scanned area A to the probe area A', and dividing by the number of atoms of the given type in the scanned image (e.g., 1 for Si and about 10 for C). The theoretical maximum count rate is given by Eq. (1), with A' substituting for A. This methodology can overestimate the experimental maximum count rate if the shell under study is delocalized over a region larger than the probe, but it provides a reasonable first approximation for the shells studied here, with the greatest error for carbon. The predicted maximum count rates for the present probe size (about 1.4 Å in diameter, i.e., 1.5 Å^2 in area) using the literature values for the cross sections, yields, DQE, and the measured beam current are ~7 counts/s for an isolated single silicon atom, ~2 counts/s for a single carbon atom, and ~28 counts/s for a single Pt atom. The correspondingly scaled count rates measured in this experiment were ~4 counts/s for one silicon atom, ~1 count/s per carbon atom, and ~14 counts/s for a Pt atom. The experimentally observed count rates are about a factor of two lower than the predicted rates for C, Si, and Pt. A factor of two is well within the uncertainty generated by using different sources for the cross sections and fluorescence yields.

The theoretical EELS total count rate for a 1.5 A^2, 60 keV electron probe centered on a carbon atom is 2.5×10^5 electrons/s. Integrating the background subtracted edges in Fig. 2, taking into account that a 100 eV integration window only captures about 60% of the total energy loss electrons and that about 90% of the carbon K-loss electrons were detected, and scaling for the time the probe spent over the atom, the measured K-shell ionization rate for a single carbon atom is 1.2×10^5 electrons/s. The ratio of the experimental EDXS and EELS rates is 8×10^{-6}, which agrees surprisingly well with the theoretical ratio $\omega^* G^* DQE = 8.0 \times 10^{-6}$. Though it is not the goal of this study, careful quantification of the EELS and

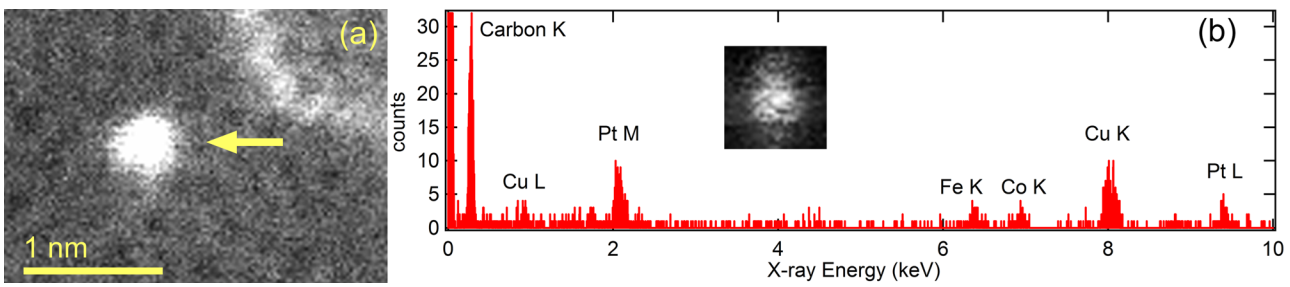

FIG. 3. (a) Single platinum atom on 3 layers carbon before x-ray spectrum acquisition and (b) x-ray spectrum with (inset) one frame from a simultaneously acquired HAADF centering movie.

EDXS signals from single atoms could provide a way to measure atomic parameters (i.e., fluorescence yields and cross sections) with unprecedented simplicity.

Given the experimental count rates, the feasibility of elemental mapping with single-atom sensitivity using EDXS can be evaluated. Using a ~1.4 Å probe, one can expect a count rate of ~4 x-rays/s for a single Si atom stationary under a 0.2 nA probe, versus ~1 count/s for a carbon atom. Without a Si atom in the scanned subframe, we observed (after scaling) ~0.16 "quasi-Si" counts/s. These are the approximate count rates observed in our preliminary single-atom elemental maps. Using simple Poisson statistics, placing the beam on a Si atom for 2 s had ~98% chance to give more than 3 Si counts, and there was <0.5% chance to get 3 counts from the background due to a graphene monolayer. So, with high statistical confidence, even just 3 counts in 2 s can be used to identify whether a given atom is a silicon atom. To identify a given atom from among 100 possible candidates requires a higher confidence, and hence longer integration time (~4 s). Of course, this is a best-case scenario of identifying isolated atoms on (or in) a graphene substrate with very little background. Even with the low count rates, elemental maps should be possible because of the low background signal of EDXS.

Regarding future improvements, a factor of ~6 improvement in count rate for the carbon K-peak is readily available by dispensing with the polymer window in front of the detector and using a larger SDD chip (60 mm^2, same outer detector tube diameter). For the Si K-peak, the same hardware change brings an improvement of about 3 times. Future improvements in detector collection efficiency could increase these figures further. For example, a collection angle of >1 sr through the use of larger detectors approaching the sample from two opposite sides may be possible, giving >30× and >15× improvements for the two peaks, respectively.

In conclusion, single atoms of silicon and platinum on a graphene substrate have been identified using EDXS. Simultaneously acquired EEL spectra gave consistent elemental identification for the Si atoms, but elemental identification of the Pt atom based on EELS proved more difficult. Using values cited in the literature for the cross sections, fluorescence yields, and detector efficiency, predicted count rates were shown to be within a factor of 2 from the experimentally measured rates. Based on these measurements, elemental mapping with single atom sensitivity using EDXS should be possible if per atom dwell times of the order of 5 s can be accommodated with a beam current of 0.2 nA in a beam of roughly 1 $Å^2$ without the atom jumping away, and probably some 10× faster in the future.

Note added in proof: During review, it has come to our attention that Suenaga *et al*. have recently and independently obtained x-ray spectra from single atoms of Er.[21]

The authors wish to thank their colleagues at Nion, Bruker Nano GmbH, and SuperSTEM for their assistance with the experiments, and general discussions. The SuperSTEM Laboratory is funded by the U.K. Engineering and Physical Sciences Research Council (EPSRC).

[1]O. L. Krivanek, M. F. Chisholm, V. Nicolosi, T. J. Pennycook, G. J. Corbin, N. Dellby, M. F. Murfitt, C. S. Own, Z. S. Szilagyi, M. P. Oxley, S. T. Pantelides, and S. J. Pennycook, Nature (London) **464**, 571 (2010).
[2]M. Varela, J. Gazquez, T. J. Pennycook, C. Magen, M. P. Oxley: S. J. Pennycook in *Scanning Transmission Electron Microscopy: Imaging and Analysis*, edited by S. J. Pennycook and P. D. Nellist (Springer, New York, 2011), Chap. 10.
[3]K. Suenaga, M. Tence, C. Mory, C. Colliex, H. Kato, T. Okazaki, H. Shinohara, K. Hirahara, S. Bandow, and S. Iijima, Science **290**, 2280 (2000).
[4]O. L. Krivanek, N. Dellby, M. F. Murfitt, M. F. Chisholm, T. J. Pennycook, K. Suenaga, and V. Nicolosi, Ultramicroscopy **110**, 935 (2010).
[5]O. L. Krivanek, M. F. Chisholm, M. F. Murfitt, and N. Dellby, "Scanning transmission electron microscopy: Albert Crewe's vision and beyond," (unpublished).
[6]Q. M. Ramasse, R. Zan, U. Bangert, N. Boukhavalov, Y. W. Son, and K. Novoselov, "Direct experimental evidence of metal-mediated graphene etching," (unpublished).
[7]M. Isaacson and D. Johnson, Ultramicroscopy **1**, 33 (1975).
[8]O. L. Krivanek, N. Dellby, and A. R. Lupini, Ultramicroscopy **78**, 1 (1999).
[9]P. E. Batson, N. Dellby, and O. L. Krivanek, Nature (London) **418**, 617 (2002).
[10]N. Dellby, N. J. Bacon, P. Hrncirik, M. F. Murfitt, G. S. Skone, Z. S. Szilagyi, and O. L. Krivanek, Eur. Phys. J.: Appl. Phys. **54**, 33505 (2011).
[11]A. J. D'Alfonso, B. Freitag, D. Klenov, and L. J. Allen, Phys. Rev. B **81**, 100101(R) (2010).
[12]M.-W. Chu, S. C. Liou, C.-P. Chang, F.-S. Choa, and C. H. Chen, Phys. Rev. Lett. **104**, 196101 (2010).
[13]D. O. Klenov and J. M. O. Zide, Appl. Phys. Lett. **99**, 141904 (2011).
[14]O. L. Krivanek, G. J. Corbin, N. Dellby, B. F. Elston, R. J. Keyse, M. F. Murfitt, C. S. Own, Z. S. Szilagyi, and J. W. Woodruff, Ultramicroscopy **108**, 179 (2008).
[15]M. Falke, private communication (2012).
[16]D. Bote, F. Salvat, A. Jablonski, and C. J. Powell, At. Data Nucl. Data Tables **95**, 871 (2009).
[17]X. Long, M. Liu, F. Ho, and X. Peng, At. Data Nucl. Data Tables **45**, 353 (1990).
[18]G. Brunner, J. Phys. B **20**, 4983 (1987).
[19]W. T. Elam, B. D. Ravel, and J. R. Sieber, Radiat. Phys. Chem. **63**,121 (2002). For this calculation, we include the possibility of ionizing an $M_{1\text{-}4}$ vacancy, undergoing a Coster-Kronig transition, and emitting an M_α (M5-N6,7) or M_β (M4-N6) x-ray. Compared to the K lines, the M line cross sections are probably less accurate due to the increased complexity and the absence of experimental data for Pt.
[20]Y. Chauhan and S. Puri, At. Data Nucl. Data Tables **94**, 38 (2008).
[21]K. Suenaga, K. Okazaki, E. Okunishi, and S. Matsumura (unpublished).